International Forum on Aeroelasticity and Structural Dynamics
IFASD 2017
25-28 June 2017 Como, Italy

A FEM-BASED APPROACH FOR NONLINEAR AEROELASTIC TRIM OF HIGHLY FLEXIBLE AIRCRAFT

Cristina Riso[1], Fausto G. Di Vincenzo[2], Markus Ritter[3], Carlos E. S. Cesnik[4], and Franco Mastroddi[1]

[1]Department of Mechanical and Aerospace Engineering
Sapienza University of Rome
via Eudossiana, 18 Roma 00184 Italy
cristina.riso@uniroma1.it

[2]MSC.Software Toulouse
Rue du Prof. Pierre Vellas, 4 Toulouse 31300 France

[3]Institute of Aeroelasticity
German Aerospace Center (DLR)
Bunsenstraße, 10 Göttingen 37073 Germany

[4]Department of Aerospace Engineering
University of Michigan
Beal Avenue, 1320 Ann Arbor 48109 Michigan (USA)

Keywords: Highly Flexible Aircraft, Nonlinear Aeroelastic Trim, Inertia Relief, Finite Element Method, Fluid-Structure Interaction.

Abstract: A novel approach is presented to compute nonlinear aeroelastic trim of highly flexible aircraft by coupling off-the-shelf solvers for structures and aerodynamics. The methodology includes an inertia relief algorithm for large displacements to perform nonlinear static analysis of unrestrained bodies, which is currently not possible in commercially available finite element codes. This feature allows to simulate free-free boundary conditions at each step of the nonlinear aeroelastic trim iterative solution sequence. The proposed approach is implemented by coupling the MSC.Nastran nonlinear structural solver SOL 400 with a three-dimensional vortex lattice method code. Loads and displacements interpolations between aerodynamic and structural grids are performed using MSC.Nastran six degree-of-freedom splines. The computational environment is tested on a beam-type model of the University of Michigan's X-HALE, a highly flexible experimental unmanned aerial vehicle for nonlinear aeroelastic flight tests. Numerical results are compared with the University of Michigan's Nonlinear Aeroelastic Simulation Toolbox and with an aeroelastic solver developed at the German Aerospace Center.

1 INTRODUCTION

Highly flexible aircraft exhibit low elastic frequencies and experience large trim deflections under typical load conditions. Rigid-body and structural dynamics are thus inherently coupled, and unique flight dynamic/aeroelastic stability, response, and control should be analyzed in statically deformed configuration rather than for the baseline structure [1]. In the past decades, unique formulations of flight dynamics and nonlinear aeroelasticity have been developed by

coupling geometrically exact beam models [2, 3] with two-dimensional potential-flow aerodynamics [4, 5]. As a result, low-order simulation tools are nowadays available to study very flexible vehicles modeled as beam-type structures [6, 7]. However, high-fidelity modeling is necessary to analyze complex configurations with sufficient detail since the early design phase. In the limit of validity of linear aeroelastic theory, finite element method (FEM) solvers are commercially available for trim, stability, and response analysis of flexible aircraft [8]. These tools are standardly used in aeroelastic design and optimization of conventional, relatively stiff configurations, for which it is adequate to assume linear aeroelastic behavior and neglect coupling between rigid-body and elastic degrees-of-freedom. Conversely, high-fidelity simulation of very flexible vehicles is still a challenge for computational aeroelasticity. Despite development of state-of-the-art methodologies for structures, aerodynamics, and flight dynamics as separate disciplines, there is still a lack of well-established multidisciplinary approaches and computational environments for integrated analysis of complex highly flexible configurations.

This paper presents a novel approach to compute nonlinear aeroelastic trim of very flexible aircraft by coupling off-the-shelf solvers for high-fidelity modeling of structures and aerodynamics. The work is a first step to extend a FEM-based simulation environment for coupled flight dynamics and aeroelasticity [9] in order to study very flexible vehicles, for which stability and response should be addressed in statically deformed configuration. The main novelties in the proposed FEM-based nonlinear aeroelastic trim methodology are 1) the use of six degree-of-freedom splines for loads and displacements interpolations between aerodynamic and structural grids; 2) a load-stepping relaxation procedure to implement a close fluid-structure coupling; and 3) an inertia relief algorithm [10–12] for large displacements to simulate free-free boundary conditions at each step of the iterative solution sequence. Indeed, clamped boundary conditions are typically assumed in the loop when using commercial displacement-based FEM solvers to compute structural deflection, since no inertia relief feature is currently available for nonlinear analyses [13]. The proposed methodology is implemented for the MSC.Nastran nonlinear structural solver SOL 400 [13] coupled with a three-dimensional vortex lattice method (VLM) code [14] used in previous studies [15, 16]. MSC.Nastran six degree-of-freedom splines generated by means of the MSC.Software Hybrid Static Aeroelasticity (HSA) Toolkit [17, 18] are used to transfer loads and interpolate displacements between structural and aerodynamic grids. The developed computational environment is applied to a beam-type model of the University of Michigan's X-HALE [19], a highly flexible experimental unmanned aerial vehicle (UAV) for nonlinear aeroelastic flight tests. Numerical results are compared with solutions from the University of Michigan's Nonlinear Aeroelastic Simulation Toolbox (UM/NAST) [7] and from a FEM-based aeroelastic solver developed at the DLR [15, 16].

The paper is organized as follows. The proposed methodology for nonlinear aeroelastic trim is presented in Sec. 2. Numerical results are discussed in Sec. 3. These include preliminary test cases to assess the core MSC.Nastran SOL 400/VLM aeroelastostatic solver and a complete nonlinear aeroelastic trim analysis of the X-HALE Reduced Risk Vehicle (RRV) [19, 20]. Concluding remarks and future work are outlined in Sec. 4.

2 NONLINEAR AEROELASTIC TRIM OF HIGHLY FLEXIBLE AIRCRAFT

Solving an aeroelastic trim problem consists of computing the combination of aerodynamic angles, control inputs, and structural deflection for which a flexible vehicle is balanced in a given equilibrium flight condition. Assuming linear elastic theory and linearized potential-flow aerodynamics, aeroelastic trim analysis of complex configurations is standardly performed

via commercial solvers that integrate displacement-based FEM structural modeling and steady Doublet Lattice Method (DLM) aerodynamics [8]. Unfortunately, no integrated software is commercially available to solve nonlinear aeroelastic trim problems. Hence, separate solvers for structures and aerodynamics must be conveniently coupled for trim analysis of complex very flexible configurations.

This section presents a novel methodology for nonlinear aeroelastic trim which is based on the coupling of off-the-shelf solvers for structures and aerodynamics to allow high-fidelity modeling of both disciplines. The proposed methodology is compared to the algorithms implemented in UM/NAST [7] and in a DLR FEM-based aeroelastic toolbox [15, 16].

2.1 Proposed algorithm

The proposed architecture for trim analysis of very flexible vehicles is shown in Fig. 1. The solution sequence consists of the Newton-Raphson loop in Fig. 1(a) and the nested nonlinear aeroelastostatic loop in Fig. 1(b). In the present work, the latter is implemented by coupling the MSC.Nastran nonlinear structural solver SOL 400 with a three-dimensional VLM code [14] developed for previous studies [15, 16]. However, the algorithm in Fig. 1(b) is applicable to generic off-the-shelf structural and aerodynamic solvers. At each iteration of the outer Newton-Raphson loop in Fig. 1(a) the nonlinear aeroelastostatic solver in Fig. 1(b) is called to obtain the structural deflection and steady aerodynamic load for the current approximation to the trim variables. These outputs are used to verify the vehicle equilibrium and, in the negative case, to update the trim variables estimates by numerically computing the system Jacobian matrix. The nonlinear aeroelastostatic solution algorithm in Fig. 1(b) is the core of the proposed methodology and consists of the following steps:

1. The aerodynamic solver is called to compute the aerodynamic load distribution on the current aerodynamic model configuration;
2. The aerodynamic load is transferred to the structural grids by means of six degree-of-freedom splines;
3. The gravity field is added to compute the residual non-balanced load resultant;
4. The resulting inertia relief load is added to aerodynamics and gravity to obtain a self-equilibrating load distribution;
5. The overall load is multiplied by a scaling factor for relaxation;
6. The structural solver is called to perform an incremental nonlinear static analysis that starts from the deformed configuration achieved at the preceding iteration and takes into account differential stiffness;
7. The incremental displacement field is interpolated by means of six degree-of-freedom splines to update the aerodynamic model;
8. The preceding steps are repeated until aeroelastostatic deflection convergence is reached.

The main novelties of the proposed algorithm are 1) the use of six degree-of-freedom splines to transfer loads and interpolate displacements between aerodynamic and structural grids; 2) the load-stepping relaxation procedure that implements a close fluid-structure coupling; and 3) the large-amplitude inertia relief algorithm to simulate free-free boundary conditions in the loop. These features are discussed in the following subsections. Note that the nonlinear aeroelastostatic solution algorithm in Fig. 1(b) can be also used as a stand-alone solver. Clamped structures can be simulated by skipping the inertia relief computations.

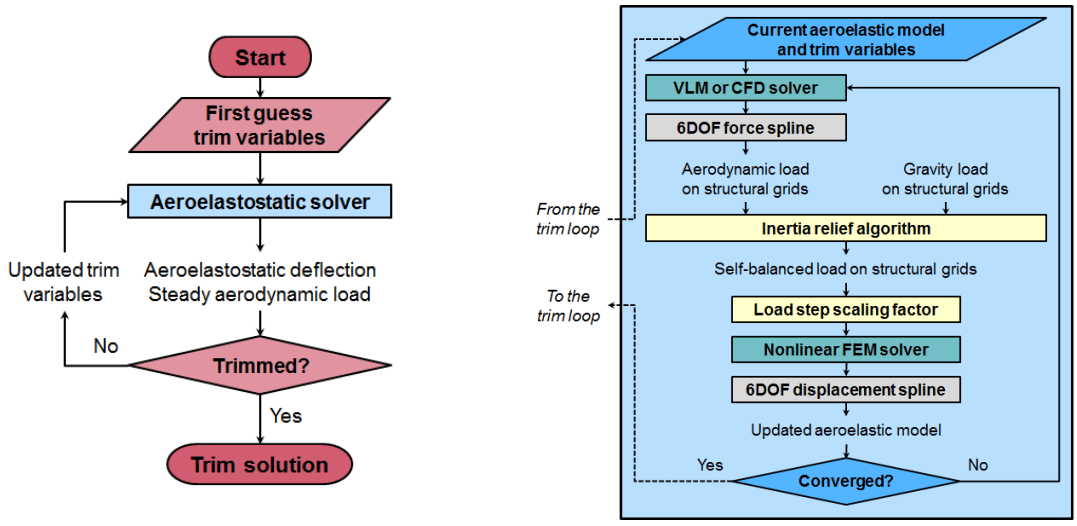

(a) Nonlinear trim solver (b) Nonlinear aeroelastostatic solver

Figure 1: Proposed architecture for trim analysis of very flexible aircraft.

2.1.1 Fluid-structure coupling

Splines standardly used in MSC.Nastran aeroelastic solvers are thought for coupling of FEM structural models with the linearized potential-flow aerodynamic models generated internally within MSC.Nastran, typically DLM models [8]. Consistently with linear aeroelastic theory, the degrees-of-freedom utilized at the coupled grids include only normal displacements for surface splines, and additionally torsional rotations for linear splines [8]. Hence, this approach may be not suitable for fluid-structure coupling with external VLM or CFD models. Indeed, the aerodynamic load defined on each body panel may be not limited to a lift force and pitching moment. In addition, all six degrees-of-freedom should be taken into account in displacements interpolation in presence of geometrically nonlinear behavior and/or to couple with viscous aerodynamic models.

To improve coupling of FEM models with external aerodynamics, an enhanced spline technology has been developed in MSC.Nastran [18]. The new splines allows the aerodynamic grids to have six degrees-of-freedom, so that all components of load and displacement fields are taken into account in the fluid-structure interaction. Both surface and linear six degree-of-freedom splines are available [17, 18], which can be used in place of the standard ones used for MSC.Nastran FEM/DLM coupling [8]. Since beam-type structural models are considered in all the present numerical studies, linear six degree-of-freedom splines are used in this work. These enable to directly interface one-dimensional structures and aerodynamic surfaces with no need to define additional leading-edge and trailing-edge grids [8]. The six degree-of-freedom splines are generated by means of the MSC.Software Hybrid Static Aeroelasticity (HSA) Toolkit [18], which enables to automatically subdivide structural and aerodynamic components in multiple spline patches with suitable overlapping in order to improve the speed and smoothness of fluid-structure coupling. The spline matrix may be updated in the loop (see Fig. 1(b)) to account for the aerodynamic and structural models deflection. The deformation of the splines axes is taken into account by defining a local coordinate system attached to a suitable structural grid for each spline patch.

2.1.2 Relaxation procedure

In case geometric nonlinearities are present in a static analysis, equilibrium of applied loads and internal stresses must be satisfied in deformed configuration, which requires an iterative solution approach. For aeroelastic analyses this implies repeated calls to the aerodynamic and structural solvers as shown in Fig. 1(b). Note that the aerodynamic load considered in each nonlinear structural analysis is evaluated on the deformed configuration achieved at the previous iteration. Therefore, the load distribution may be not consistent with the updated model in presence of large incremental deflections. In the proposed algorithm, this remark also applies to the inertia relief loads that are included in the loop to simulate free-free boundary conditions. Indeed, the inertia relief load distribution depends on the non-balanced force and moment resultant of aerodynamics and gravity and on the model rigid-body mass matrix. All these quantities vary in the loop due to structural deflection. Moreover, follower-force effects must be taken into account in a nonlinear solution. In MSC.Nastran SOL 400, follower forces and moments can be implemented by means of specific entries [13, 17]. However, these require to locally define loads orientation in terms of suitably located grids [17], which may make implementation of follower forces cumbersome for complex distributions.

In order to overcome these problems, a close fluid-structure coupling is implemented in the nonlinear aeroelastostatic solver based on the load-stepping relaxation procedure shown in Fig. 1(b). The structure is loaded incrementally in n_s fluid-structure iterations, corresponding to a load step size $1/n_s$. Each nonlinear structural analysis starts from the deformed configuration achieved at the preceding step. The load field applied to the structure in the first n_s iterations is multiplied by an increasing scaling factor j/n_s ($j = 1, \ldots, n_s$). Hence, n_s iterations of the aeroelastic static loop are necessary to take the structure from an unloaded to the fully loaded condition. The aerodynamic and inertia relief loads are recomputed at each iteration on the updated model to replace the preceding distributions, and the scaling factor for the overall applied load increases until it becomes 1. At this point n_s iterations of the aeroelastostatic loop in Fig. 1(b) have been performed, so that the structure is in a fully loaded condition. However, further iterations may be still necessary for convergence. Additional n_a fluid-structure iterations are thus performed until the aeroelastostatic deflection converges using a load scaling factor always equal to 1. The total number of fluid-structure iterations in the loop is thus $n_i = n_s + n_a$, obtained by summing n_s incremental load steps and n_a additional iterations performed after the structure is fully loaded.

The proposed load-stepping relaxation procedure improves stability and accuracy of the aeroelastostatic solution algorithm by implementing a close fluid-structure coupling, which may also save computational time (see Subsecs. 3.1.2 and 3.2). Indeed, the step size can be tailored to each test case to keep incremental deflections moderate between subsequent fluid-structure iterations, which improves the algorithm robustness and speed. This also allows to assume the aerodynamic load as non-follower within each iteration, since incremental deflections are limited by the load stepping and follower-force effects can be thus accurately simulated by updating the load at each call to the structural solver. Hence, standard non-follower force and moment entries [17] can be used to input aerodynamic loads in the MSC.Nastran SOL 400.

2.1.3 Inertia relief algorithm

Conventional displacement-based FEM static analysis cannot be performed on an unrestrained body, since the model stiffness matrix becomes singular in this condition. However, commercial

displacement-based FEM solvers use the inertia relief concept [10–12] to simulate free-free structures in linear structural and aeroelastic analyses [8, 12]. If a free structure is subjected to a non-balanced load field, a rigid-body acceleration occurs. When using inertia relief, apparent inertial loads are added in the analysis to obtain an overall self-balancing load distribution. This allows to constrain the model at an arbitrarily selected grid for the purpose of stiffness matrix inversion while still simulating free-free boundary conditions, as the constraint gives zero reaction in presence of a self-balancing load field. In this case, elastic deflections obtained with different choices of the constrained grid can be superimposed by means of a rigid-body displacement, so that they represent the unique deformed state of the unrestrained structure under the original non-balanced load [21].

Unfortunately, no inertia relief mechanism is currently implemented for nonlinear static and dynamic analyses in commercially available FEM solvers [13]. As a consequence, clamped boundary conditions must be assumed. In the case of nonlinear aeroelastic trim analyses, the applied load distribution is by definition self-balancing when the trim condition is achieved, so that the converged aeroelastostatic deflection is representative of an unrestrained structure even if the model is clamped at some grid for stiffness matrix inversion. However, free-free boundary conditions are not simulated in the nonlinear structural analyses performed in the trim loop unless apparent inertial loads are taken into account. Indeed, aerodynamics and gravity do not give a self-balancing load field until the trim condition is verified, which gives a non-zero reaction experienced at the constrained grid if the inertia relief concept is not applied. This may lead to larger deflections within the loop while converging to the trim solution, which may negatively affect algorithm stability, accuracy, and computational time (see Subsec. 3.2).

In order to simulate free-free boundary conditions at each step of the nonlinear aeroelastic trim solution sequence, an inertial relief algorithm for large displacements is implemented externally to MSC.Nastran SOL 400 as shown in Fig. 1(b). The algorithm extends the inertial relief feature implemented in MSC.Nastran linear aeroelastic solvers [8, 11, 12] by iteratively recomputing and updating inertia relief loads in the loop. This is necessary for nonlinear problems since 1) aerodynamic loads are updated in the loop; 2) the application points of aerodynamic and gravity loads move; and 3) the model mass distribution varies with structural deflection.

The proposed inertia relief algorithm is implemented as follows. A fixity structural grid is chosen that experiences zero displacement in the nonlinear aeroelastic trim solution, so that the relative displacement field is computed. The fixity grid position in the FEM model in the assumed coordinate system is given by $\underline{\mathbf{x}}_{\mathsf{c}}$ and remains constant in the iterative solution process. At the jth iteration of the nonlinear aeroelastostatic loop, the force and moment resultants of aerodynamics and gravity with respect to the fixity grid are given by:

$$\underline{\mathbf{F}}^{\mathsf{j}}_{\mathsf{tot}} = \sum_{\mathsf{i}=1}^{\mathsf{N}} \left(\underline{\mathbf{f}}^{\mathsf{j}}_{\mathsf{i,a}} + \underline{\mathbf{f}}^{\mathsf{j}}_{\mathsf{i,g}} \right) \qquad \underline{\mathbf{M}}^{\mathsf{j}}_{\mathsf{tot}} = \sum_{\mathsf{i}=1}^{\mathsf{N}} \left[\left(\underline{\mathbf{x}}^{\mathsf{j}}_{\mathsf{i}} - \underline{\mathbf{x}}_{\mathsf{c}} \right) \times \left(\underline{\mathbf{f}}^{\mathsf{j}}_{\mathsf{i,a}} + \underline{\mathbf{f}}^{\mathsf{j}}_{\mathsf{i,g}} \right) + \underline{\mathbf{m}}^{\mathsf{j}}_{\mathsf{i,a}} \right] \tag{1}$$

In the above equation, the quantities $\underline{\mathbf{f}}^{\mathsf{j}}_{\mathsf{i,a}}$, $\underline{\mathbf{f}}^{\mathsf{j}}_{\mathsf{i,g}}$, and $\underline{\mathbf{m}}^{\mathsf{j}}_{\mathsf{i,a}}$ are respectively the pin aerodynamic force, gravity force, and aerodynamic moment applied at the jth iteration on the ith grid of current position $\underline{\mathbf{x}}^{\mathsf{j}}_{\mathsf{i}}$. The apparent rigid-body translational and rotational accelerations due to the net force and moment resultants in Eq. (1) are recovered from:

$$\underline{\underline{\mathbf{M}}}^{\mathsf{j}}_{\mathsf{rb}} \left\{ \begin{array}{c} \underline{\mathbf{a}}^{\mathsf{j}}_{\mathsf{rb,t}} \\ \underline{\mathbf{a}}^{\mathsf{j}}_{\mathsf{rb,r}} \end{array} \right\} = - \left\{ \begin{array}{c} \underline{\mathbf{F}}^{\mathsf{j}}_{\mathsf{tot}} \\ \underline{\mathbf{M}}^{\mathsf{j}}_{\mathsf{tot}} \end{array} \right\} \tag{2}$$

where $\underline{\underline{\mathbf{M}}}^{\mathsf{j}}_{\mathsf{rb}}$ is the 6×6 model rigid-body mass matrix with respect to the fixity grid evaluated at the jth iteration. The acceleration loads due to the apparent accelerations in Eq. (2) give the inertia relief load distribution that is added to aerodynamics and gravity as shown in Fig. 1(b). With this approach, the overall load distribution applied to the structure is self-balancing at each iteration even if the trim condition is not satisfied yet. Consequently, free-free boundary conditions are simulated in the loop. Indeed, although the fixity grid is clamped for stiffness matrix inversion, no constraint is actually experienced by the model since there is no reaction in presence of a self-balancing load distribution. Besides the present use in the nonlinear aeroelastic trim architecture shown in Fig. 1, note that the proposed inertia relief algorithm can be also applied to simulate free-free boundary conditions in generic nonlinear static and dynamic analyses.

2.2 Comparison with existing algorithms

In the present work, numerical results obtained with the proposed methodology are compared with predictions from the nonlinear aeroelastic trim solvers implemented in UM/NAST [7] and in an aeroelastic toolbox developed at the DLR [15, 16]. The main features of the examined approaches are summarized below and in Tab. 1.

Nonlinear structures are modeled in UM/NAST using a strain-based geometrically exact beam formulation [3]. Nonlinear aeroelastic trim is performed by either solving the force/moment equilibrium or forcing zero linear and angular accelerations at the origin of the body reference system. This is accomplished by means of an outer Newton-Raphson loop as the one shown in Fig. 1(a) and an inner nonlinear aeroelastostatic solver that couples the strain-based beam formulation with strip theory or, more recently, with a three-dimensional VLM code [14] along with gravity loads and load factors. The aerodynamic model and loads are updated at each aeroelastostatic iteration by recovering structural displacements from strains. Fluid-structure coupling is performed by transferring each aerodynamic chordwise load distribution to the corresponding beam axis location and by recovering the rigid-body cross-sectional displacement field from the beam axis deflection. Inertia relief is not necessary in UM/NAST since the model stiffness matrix is always definite positive in the strain-based formulation.

The DLR aeroelastic toolbox is a FEM-based simulation environment that allows analysis of complex configurations using linear, reduced-order, or fully nonlinear structural formulations [15, 16]. The nonlinear aeroelastic trim solver consists of a main Newton-Raphson loop as the one in Fig. 1(a) and a nested nonlinear aeroelastostatic loop based on MSC.Nastran SOL 400 coupled with the VLM code [14] considered in Ref. [15, 16]. The same code is used to implement the proposed methodology and it has been also interfaced with UM/NAST to allow three-dimensional aerodynamic modeling. Fluid-structure coupling is performed using Radial Basis Functions (RBF) and, for beam-type FEMs, the coupling model approach [15, 16] to expand one-dimensional structures. No load-stepping relaxation procedure is currently implemented in the loop. Each MSC.Nastran SOL 400 nonlinear static analysis starts from the undeformed configuration, but considers the aerodynamic load distribution computed on the updated VLM model. A structural grid is clamped in the loop to invert the FEM stiffness matrix.

3 NUMERICAL RESULTS

Preliminary analyses to assess the core nonlinear aeroelastostatic solver are discussed in Subsec. 3.1. The proposed nonlinear aeroelastic trim methodology is applied to the X-HALE RRV [19, 20] in Subsec. 3.2.

Table 1: Main features of the implemented nonlinear aeroelastic trim solver based on the solution algorithm proposed in Fig. 1 and comparison with the UM/NAST and DLR solvers.

Feature	**Present solver**	**UM/NAST solver**	**DLR solver**
Structural modeling	Complex FEM	Strain-based beam	Complex FEM
Aerodynamic modeling	VLM	VLM	VLM
Coupling approach	6 DOF splines	Section-based	RBF
Relaxation	Yes	No	No
Inertia relief	Yes	Not applicable	No

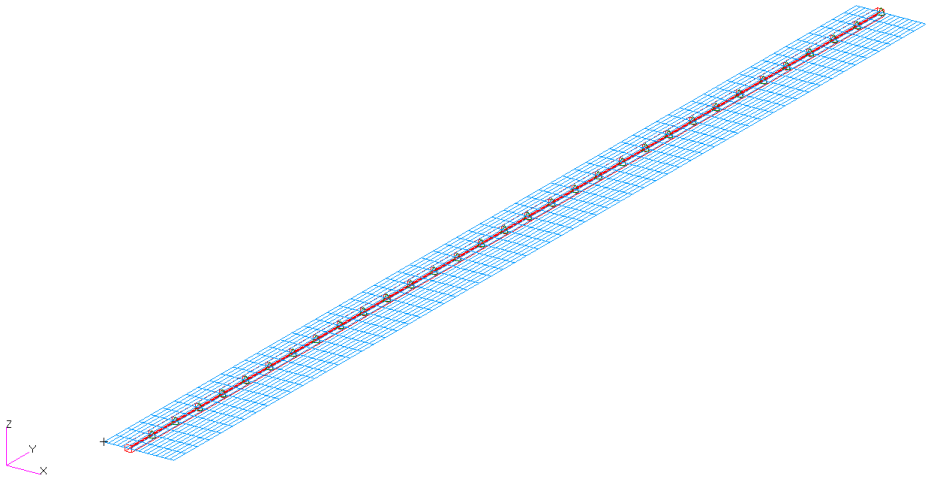

Figure 2: Highly flexible 16-meter wing aeroelastic model [15].

3.1 Assessment of the nonlinear aeroelastostatic solver

The nonlinear aeroelastostatic solution algorithm in Fig. 1(b) is implemented for MSC.Nastran SOL 400 coupled with the VLM code used in Refs. [15, 16]. Fluid-structure coupling is performed via MSC.Nastran six degree-of-freedom splines [17] generated by means of the MSC.Software HSA Toolkit [18]. The developed nonlinear aeroelastostatic solver is assessed by computing the response of clamped structures at prescribed free-stream velocity and angle of attack. The inertia relief algorithm is switched off in the solution sequence in Fig. 1(b) to implement clamped boundary conditions. Two test cases of increasing complexity are considered: 1) the highly flexible 16-meter wing studied in Ref. [15]; and 2) the X-HALE RRV analyzed in Ref. [16]. Beam-type FEM models are considered for both applications to directly compare the deflections with UM/NAST. The results are also compared with the MSC.Nastran SOL 400/VLM nonlinear aeroelastostatic solver of the DLR toolbox.

3.1.1 Test case 1: 16-meter beam

The first test case is the highly flexible 16-meter wing studied in Ref. [15]. Nonlinear aeroelastostatic analyses are carried out using 1) the present MSC.Nastran SOL 400/VLM solver; 2) the UM/NAST solver based on strip-theory aerodynamics corrected with weighting factors [15]; 3) the UM/NAST solver based on VLM aerodynamics; and 4) the MSC.Nastran SOL 400/VLM solver of the DLR toolbox. The aeroelastic model used for the present computations is shown in

Table 2: Nonlinear aeroelastostatic response of the 16-meter wing at sea level, $U = 40$ m/s, and $\alpha = 5°$ with no gravity: tip vertical displacement over semispan, computational time, and number of iterations using the proposed approach with different step size.

Step size (%)	$\overline{u}_{z_{\text{tip}}}$ (%)	$\Delta\overline{u}_{z_{\text{tip}}}$ (%)	Time (s)	n_s	n_a	n_i
100	20.3053	–	125.52	1	4	5
50	20.2622	-0.2124	176.44	2	4	6
20	20.2147	-0.2343	206.60	5	4	9
10	20.1959	-0.0931	264.00	10	3	13
5	20.1862	-0.0481	512.84	20	3	23

Table 3: Nonlinear aeroelastostatic response of the 16-meter wing at sea level, $U = 40$ m/s, and $\alpha = 3°, 4°, 5°$ with no gravity: tip vertical displacement over semispan (%) obtained using the proposed approach, UM/NAST with strip theory [13], UM/NAST with VLM, and the DLR toolbox.

	$\alpha = 3°$	$\alpha = 4°$	$\alpha = 5°$
Proposed approach	12.5996	16.5067	20.1959
UM/NAST with VLM	12.3633	16.1815	19.7798
UM/NAST with strip theory	12.5964	16.4977	20.1787
DLR toolbox	12.6233	16.5733	20.3294

Fig. 2 and consists of a single-member beam-type structure with quadratically varying stiffness properties coupled with a unit-chord rectangular lifting surface [15].

The aeroelastostatic response of the 16-meter wing is studied at sea level for fixed free-stream velocity $U = 40$ m/s and increasing angle of attack $\alpha = 3°, 4°, 5°$. Gravity is not taken into account. In order to choose the number of load steps for the relaxation procedure in Fig. 1(b), a preliminary sensitivity analysis is carried out for $\alpha = 5°$ by performing multiple computations with different step size. The variation of tip vertical displacement over semispan, computational time, and number of iterations with the step size is summarized in Tab. 2. The tip vertical displacement decreases by reducing the step size, but no practical change is found for step size below 10%. Hence, this value is assumed for all the analyses. For this test case, the total number of iterations n_i increases by reducing the step size due to the consequent increasing

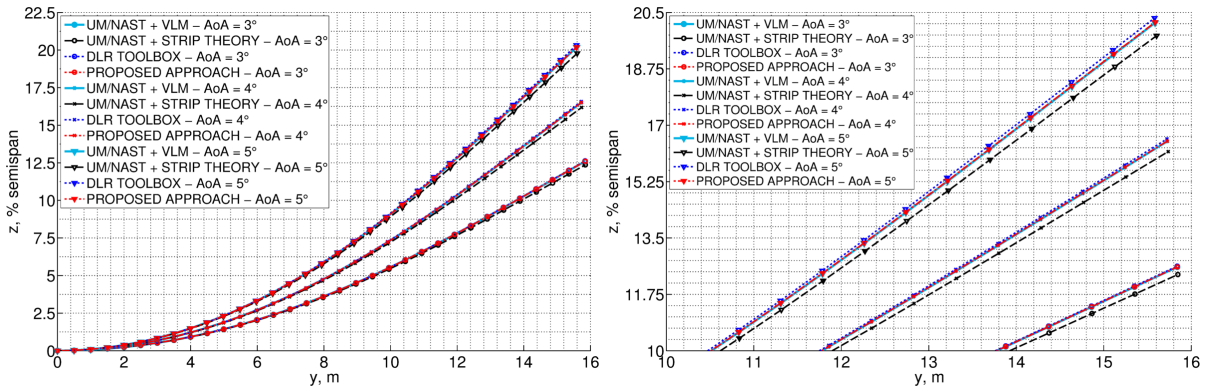

Figure 3: Nonlinear aeroelastostatic response of the 16-meter wing at sea level, $U = 40$ m/s and $\alpha = 3°, 4°, 5°$ with no gravity: deformed configuration in the vertical plane obtained using the proposed approach, UM/NAST with strip theory [13], UM/NAST with VLM, and the DLR toolbox.

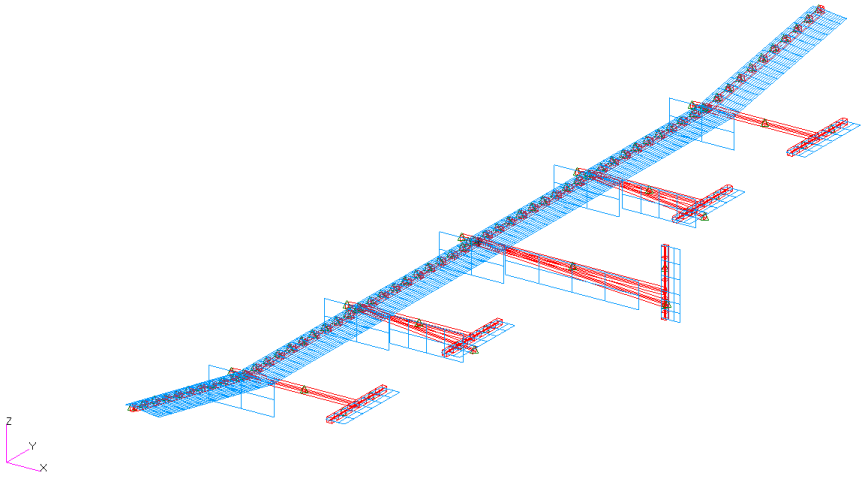

Figure 4: X-HALE RRV aeroelastic model [16].

number of load steps. However, the n_a additional iterations for convergence after the structure is fully loaded decrease from 4 to 3 for smaller step size. This behavior is expected since a closer fluid-structure coupling is implemented by reducing the step size, which gives a smoother approaching of the converged solution. This does not result in smaller computational time for this simple test case since the analysis converges fast even without load-stepping, and the number of iterations necessary after the structure is fully loaded shows just a slight dependency on the step size (see Tab. 2). However, the load-stepping relaxation procedure may allow to save computational time for more complex configurations as shown in Subsec. 3.1.2.

The aeroelastostatic deflection in the vertical plane obtained for $\alpha = 3°, 4°, 5°$ with different approaches are compared in Fig. 3. The tip vertical deflections over semispan are also compared in Tab. 3. The solutions predicted with the proposed approach match the UM/NAST results based on VLM aerodynamics at all the angles of attack. The DLR toolbox solution practically lies on top of the previous ones, just showing a 0.65% larger tip vertical displacement for $\alpha = 5°$. The UM/NAST deflection based on strip-theory aerodynamic is always smaller than with VLM. The relative difference in the tip vertical displacement increases from 1.85% to 2% with the angle of attack. This is justified by the larger deflection experienced at higher angle of attack, since the weighting factors used to tune the strip-theory aerodynamic load distribution are evaluated for the undeformed wing [15].

3.1.2 Test case 2: X-HALE RRV

The second test case is the X-HALE RRV studied in Ref. [16] and also considered for the nonlinear aeroelastic trim analyses. This case study enables to assess the nonlinear aeroelastostatic solver for a realistic configuration composed by multiple structural members and interacting aerodynamic surfaces. Nonlinear aeroelastostatic analyses are carried out using 1) the present MSC.Nastran SOL 400/VLM solver; 2) the UM/NAST solver based on VLM aerodynamics; and 3) the MSC.Nastran SOL 400/VLM solver of the DLR toolbox. The UM/NAST results based on strip-theory aerodynamics in Ref. [16] are not considered for comparison since strip theory does not take into account mutual interactions between aerodynamic surfaces, which are significant for the X-HALE RRV. The aeroelastic model used for the present computations is

Table 4: Nonlinear aeroelastostatic response of the X-HALE RRV for $\rho = 1.22161$ kg/m^3, $U = 16$ m/s, and $\alpha = 1^\circ$ with gravity: right-half wing tip vertical displacement over semispan, computational time, and number of iterations using the proposed approach with different step size.

Step size (%)	$\overline{u}_{z_{\text{tip}}}$ (%)	$\Delta\overline{u}_{z_{\text{tip}}}$ (%)	Time (s)	n_s	n_a	n_i
100	17.4326	–	1093.96	1	28	29
50	16.7863	-0.6463	727.21	2	20	22
20	16.4141	-0.3722	808.01	5	19	24
10	16.2952	-0.1189	931.56	10	17	27
5	16.2368	-0.0584	1227.02	20	15	35

Table 5: Nonlinear aeroelastostatic response of the X-HALE RRV for $\rho = 1.22161$ kg/m^3, $U = 16$ m/s, and $\alpha = 0^\circ, 0.5^\circ, 1^\circ$ with gravity: right half-wing tip vertical displacement over semispan (%) obtained using the proposed approach, UM/NAST with VLM, and the DLR toolbox.

	$\alpha = 0^\circ$	$\alpha = 0.5^\circ$	$\alpha = 1^\circ$
Proposed approach	11.7419	14.0734	16.2952
UM/NAST with VLM	11.8773	14.3971	16.8117
DLR toolbox	11.6878	14.0520	16.3138

shown in Fig. 4 and consists of a flexible beam-type member to model the wing elastic axis and rigid bars to represent booms, tails, pods, and fins. The wing is divided in six unit segments, with the outer ones presenting a 10° positive dihedral. The wing aerodynamic model features a reverse-camber EMX07 airfoil and has an incidence of 5° with respect to the horizontal axis. Flat-plate surfaces are used to model pods, fins, and tails. Further details on the X-HALE RRV configuration and model are found in Refs. [16, 19, 20]

The aeroelastostatic response of the X-HALE RRV is studied for $\rho = 1.22161$ kg/m^3, fixed free-stream velocity $U = 16$ m/s and increasing angle of attack $\alpha = 0^\circ, 0.5^\circ, 1^\circ$. Gravity is included in the analysis ($g = 9.80665$ m/s^2). Solution sensitivity to the step size is preliminarily analyzed for $\alpha = 1^\circ$ as summarized in Tab. 4. The tip vertical displacement decreases by reducing the step size as found for the 16-meter wing, although a higher sensitivity to the load path is observed for this more complex test case. In contrast with what observed for the 16-meter

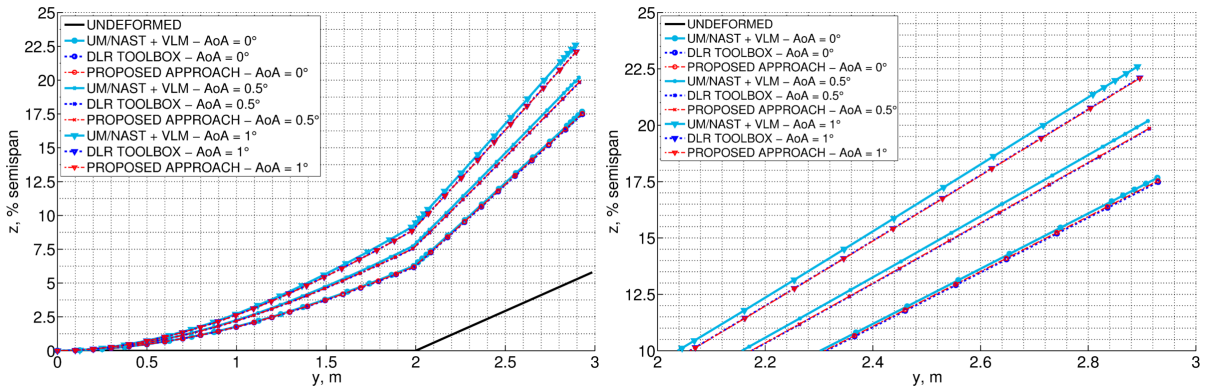

Figure 5: Nonlinear aeroelastostatic response of the X-HALE RRV for $\rho = 1.22161$ kg/m^3, $U = 16$ m/s and $\alpha = 0^\circ, 0.5^\circ, 1^\circ$ with gravity: right half-wing deformed configuration in the vertical obtained using the proposed approach, UM/NAST with VLM, and the DLR toolbox.

wing, note that computational time does not monotonically increase by reducing the step size for the X-HALE RRV. Indeed, it first decrease by reducing the step size from 100% (no relaxation) to 50%, then it increases for further reductions. However, the time necessary to complete the analysis with load steps of 10% is still smaller than with no relaxation. This occurs because the number of load-step iterations n_s increases by reducing the step size, but the additional $n_a = n_i - n_s$ iterations performed after the structure is fully loaded significantly decrease from 28 to 15 (see Tab. 4). Since incremental deflections are very small after taking the structure to a fully loaded condition, the last n_a iterations are faster than the first n_s ones associated with load steps. As a consequence, the computational time necessary with relaxation is smaller than with no relaxation for step size not below 10%, since in this case most of the total iterations are performed after the structure is fully loaded ($n_s < n_a$). Conversely, computational time increases with respect to the case of no relaxation for step size below 10%, since in this case most of the total iterations are load steps ($n_s > n_a$). This behavior is not observed for the 16-meter wing, since the nonlinear aeroelastic analyses are very fast due to the model simplicity and the number of iterations performed after the structure is fully loaded shows just a slight dependency on the step size (see Tab. 2). Taking into account the above remarks and that the X-HALE aeroelastostatic response practically does not change for step size below 10% (see Tab. 4), this value is assumed for all the analyses. For $\alpha = 1^\circ$, the analysis with step size equal to 10% is 15% faster than with no relaxation (see Tab. 4).

The aeroelastostatic results obtained for $\alpha = 0^\circ, 0.5^\circ, 1^\circ$ with different solvers are compared in Fig. 5 and Tab. 5. The responses predicted with the proposed approach and the DLR toolbox practically overlap for all the angles of attack, whereas UM/NAST predicts larger displacements. The difference at tip increases from 1.1% to 3% with the angle of attack. This fact may be justified by considering that a section-based fluid-structure coupling is used in UM/NAST (see Subsec. 2.2), so that the load transferred to each structural grid is only influenced by the aerodynamic grids in a close neighborhood. Conversely, the fluid-structure coupling approaches used in the present solver and in the DLR toolbox involve regions of the aerodynamic and structural models, so that mutual influence between cross-sections is taken into account in load transferal.

Additional analyses performed on the X-HALE RRV for $\alpha = 1^\circ$ and increasing free-stream velocity have pointed out that for larger nonlinearities the proposed solution algorithm is not stable in the absence of relaxation (step size equal to 100%), and that the DLR solver cannot achieve a convergent solution as well. This issue may be critical in presence of very large nonlinearities. Further investigation on the solution sensitivity to the load path in terms of stability, accuracy, and computational time for highly geometrically nonlinear behavior will be carried out in a future work.

3.2 Nonlinear aeroelastic trim of the X-HALE

A complete longitudinal nonlinear aeroelastic trim analysis of the X-HALE RRV is performed for level flight at $\rho = 1.22161$ kg/m^3 and $U = 16$ m/s, which is a typical operative condition for the vehicle [19, 20]. The aeroelastic model considered for trim is the same as described in Subsec. 3.1.2, with the horizontal tails modeled as control surfaces to satisfy pitch equilibrium. The nonlinear aeroelastic trim analysis is carried out using 1) the present solver composed by the outer Newton-Raphson loop in Fig. 1(a) and the nonlinear aeroelastostatic solver assessed in Subsec. 3.1; 2) the UM/NAST nonlinear aeroelastic trim based on VLM aerodynamics; and 3) the nonlinear aeroelastic trim solver of the DLR toolbox. The computation of inertia relief loads

is activated in the present solver to simulate free-free boundary conditions at each iteration. The fixity grid for the inertia relief algorithm in Subsec. 2.1.3 is chosen at wing beam axis centerline, so that the aeroelastic trim deflection is evaluated relatively to this grid. With this choice the result can be directly compared with the DLR toolbox solution, which is computed by clamping the same grid in the loop in order to invert the model stiffness matrix. The structural deflection given by UM/NAST is also referred to this grid, but this is computed with no need to either impose a constraint or use inertia relief since the strain-based stiffness matrix is always definite positive. Since the X-HALE RRV experiences tip deflections of about 5% semispan in the examined flight condition [16, 19], a larger step size equal to 20% is assumed in the present solver for the trim analysis in place of the smaller value 10% used in Subsec. 3.1.2. Indeed, the latter does not give any change in the solution for deflections of this order of magnitude. With this choice, the trim solution converges 10% faster than with no relaxation (step size equal to 100%). Linear aeroelastic trim predictions are also obtained for comparison using the MSC.Nastran SOL 144 solver [8], which performs a one-shot fully linear aeroelastic trim analysis based on steady DLM aerodynamics. Since only flat-plate surfaces can be modeled via DLM, a correction to account for the X-HALE RRV wing incidence and camber must be included in the analysis [8]. Two approaches are considered for this purpose. The first one is to input a downwash distribution to take into account rotation of the DLM panels normal vectors due to incidence and camber in the aerodynamic boundary conditions [8, 17]. The second approach is to include an external load field to take into account the aerodynamic loads experienced at zero angle of attack, which are not captured by DLM. In this work, the supplied external load is given by the VLM aerodynamic load distribution on the undeformed vehicle at the examined trim velocity, zero angle of attack, and zero tails deflection.

The aeroelastic trim results obtained with different approaches are summarized in Tab. 6, while the trim right half-wing deflections in the vertical plane are compared in Fig. 6. The true-scale trim deformed configuration and the VLM force distribution are shown in Fig. 7. A better agreement in terms of structural deflection and tails rotation is found between the results from the present solver and the DLR toolbox, whereas the UM/NAST and DLR toolbox trim angles of attack are slightly closer. However, differences between UM/NAST and the other approaches could be expected from the ones discussed in Subsec. 3.1.2. Since the X-HALE RRV experiences a moderate deflection in the examined flight condition [16, 19], a good agreement between nonlinear and linear predictions is found. A better matching of the VLM-based results is achieved by accounting for wing incidence and camber using the external aerodynamic load input than the downwash input [8,17]. This is justified by considering that only the aerodynamic boundary conditions are influenced by downwash input, which does not alter the DLM model geometry and thus the computation of the Aerodynamic Influence Coefficient (AIC) matrix. Conversely, the external load included in MSC.Nastran SOL 144 to account for aerodynamic loads at zero angle of attack is based on the actual VLM model geometry, and thus provides a more accurate modeling of incidence and camber effects.

In order to point out the advantage of including inertia relief in the trim loop when using a commercial (displacement-based) FEM solver compute structural deflection, an additional analysis is carried out with the present methodology by assuming the same parameters as before but switching the inertia relief algorithm off (see Fig. 1). The result is compared with the one computed using inertia relief to focus only on the effect of this feature, which cannot be isolated by comparing the present solution with the DLR toolbox one. Free-free boundary conditions are simulated at each iteration in the present solver when the inertia relief algorithm is activated, whereas clamped boundary conditions are used in the loop when inertia relief is off. Note that

Table 6: Aeroelastic trim of the X-HALE RRV for level flight at $\rho = 1.22161$ kg/m^3 and $U = 16$ m/s: right half-wing tip displacement over semispan, angle of attack, and tails deflection obtained using the proposed approach (inertia relief in the loop), UM/NAST with VLM, the DLR toolbox, and MSC.Nastran SOL 144 [8].

	$\overline{u}_{z_{tip}}$ (%)	α (deg)	δ_e (deg)
Proposed approach	5.0696	0.7503	2.4162
DLR toolbox	4.9992	0.7853	2.4716
UM/NAST	4.7010	0.7922	2.6162
MSC.Nastran SOL 144 with external load input	4.8966	0.7330	2.5962
MSC.Nastran SOL 144 with downwash input	4.6096	0.7155	2.6099

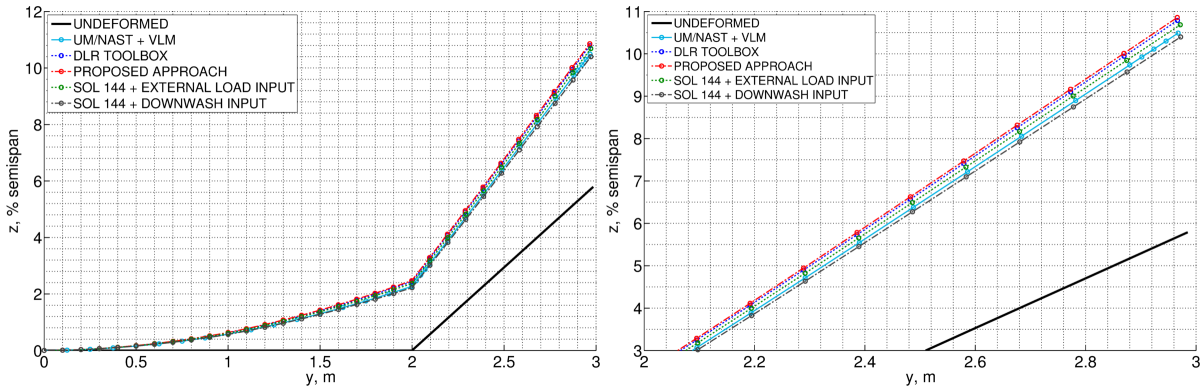

Figure 6: Aeroelastic trim of the X-HALE RRV for level flight at $\rho = 1.22161$ kg/m^3 and $U = 16$ m/s: right half-wing deformed configuration in the vertical plane obtained using the proposed approach (inertia relief in the loop), UM/NAST with VLM, the DLR toolbox, and MSC.Nastran SOL 144 [8].

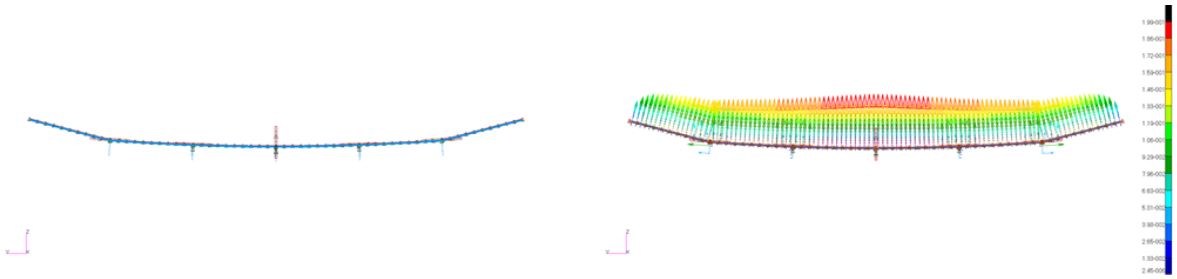

Figure 7: Aeroelastic trim of the X-HALE RRV for level flight at $\rho = 1.22161$ kg/m^3 and $U = 16$ m/s: vehicle deformed configuration in the vertical plane in true scale and VLM aerodynamic force distribution obtained with the proposed approach (inertia relief in the loop).

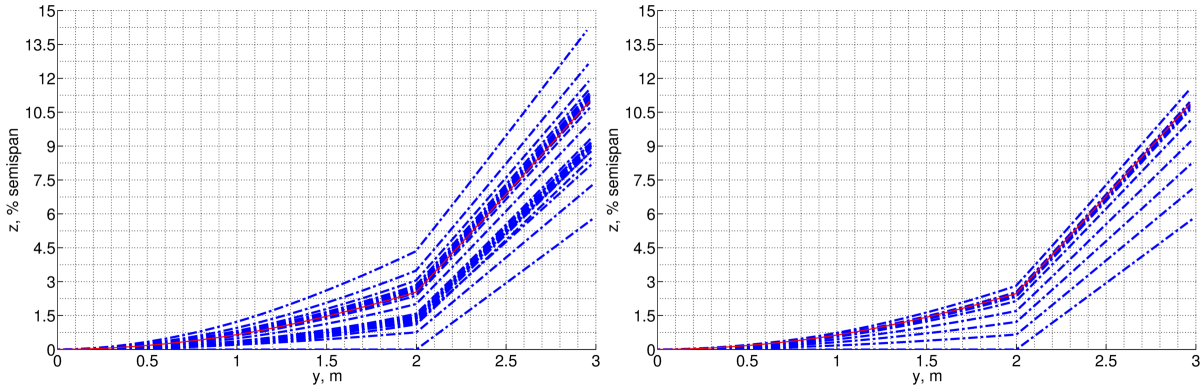

(a) Inertia relief off (b) Inertia relief on

Figure 8: Aeroelastic trim of the X-HALE RRV for level flight at $\rho = 1.22161$ kg/m^3 and $U = 16$ m/s: right half-wing deformed configuration in the vertical plane at each iteration of the trim loop (blue) and converged solution (red) obtained using the proposed approach with inertia relief off/on.

Table 7: Aeroelastic trim of the X-HALE RRV for level flight at $\rho = 1.22161$ kg/m^3 and $U = 16$ m/s: right half-wing tip vertical displacement over semispan, angle of attack, tails deflection, computational time, and number of iterations using the proposed approach with inertia relief off/on.

	$\overline{u}_{z_{\text{tip}}}$ (%)	α (deg)	δ_e (deg)	Time (s)	n_i
Inrel off	5.1898	0.7203	2.4414	2511.21	87
Inrel on	5.0696	0.7503	2.4162	1111.14	32
Δ%	-0.12	4.16	-1.03	-55.75	-63.22

the converged solution is in both cases representative of an unrestrained vehicle, since the aerodynamic and gravity load fields give a self-balancing distribution at trim and no reactive load is thus experienced at the clamped grid. However, the path followed to achieve the converged solution is different in the two cases, since aerodynamics and gravity are not self-balancing in the loop.

The intermediate right half-wing deflections in the loop (blue) and the converged solution (red) obtained with inertia relief off/on are shown in Fig. 8. The trim right half-wing tip vertical displacement over semispan, angle of attack, tails deflection, computational time, and number of fluid-structure iterations are compared in Tab. 7. Figure 8 shows that a more regular convergence to the trim solution is achieved using inertia relief, which results in a 56% computational time saving with respect to the case of inertia relief off. This behavior is justified by considering that a physics-based load path is followed using inertia relief, as the structure is simulated as unrestrained while it incrementally deflects toward the trim solution. Indeed, aerodynamics and gravity do not give a self-balancing load field in the loop, since the trim condition is not satisfied yet. Therefore, the model experiences a non-zero reaction at the clamped grid when the inertia relief algorithm is switched off. Conversely, although a grid is still kept fixed when the inertia relief algorithm is activated, in this case the model does not experience any constraint. The apparent inertial loads are added to aerodynamics and gravity in each nonlinear structural analysis, so that the structure is always subjected to a self-balancing load distribution and no reactive load is consequently experienced at the fixed grid. This results in smaller deflections in the loop as shown in Fig. 8, which saves fluid-structure iterations and thus computational time as shown in Tab. 7. The trim solutions obtained with inertia relief off/on are moderately

different, which is justified by considering that the stiffness matrix is updated in the loop and it is thus sensitive to the load path. The main difference is observed in the trim angle of attack, whereas the obtained aeroelastostatic deflections practically overlap. Note that including an inertia relief algorithm in the loop to simulate free-free boundary conditions at any iteration is of concern only when using a displacement-based FEM solver (like standard commercial FEM solvers) to compute structural deflection. Indeed, the model stiffness matrix is always definite positive when the independent variables are element strains rather than nodal displacements. For this reason, simulating unrestrained bodies is not critical in the case of a strain-based finite element analysis.

4 CONCLUDING REMARKS

A novel approach has been presented to compute nonlinear aeroelastic trim of highly flexible aircraft by coupling off-the-shelf solvers for high-fidelity modeling of structures and aerodynamics. The main features of the proposed trim methodology are 1) the use of six degree-of-freedom splines for loads and displacements interpolation between aerodynamic and structural grids; 2) a load-stepping relaxation procedure to implement a close fluid-structural coupling; and 3) a large-amplitude inertia relief algorithm to simulate free-free boundary conditions in the loop. The proposed approach has been implemented for MSC.Nastran SOL 400 coupled with a three-dimensional VLM code using six degree-of-freedom splines. The developed computational environment has been assessed by performing both nonlinear aeroelastic static analyses of a 16-meter wing and of the University of Michigan's X-HALE RRV at different prescribed flight conditions and a complete nonlinear aeroelastic trim analysis of the latter configuration. Beam-type FEM models have been considered in all the numerical studies in order to directly compare the results with UM/NAST. The results have been also compared with a MSC.Nastran SOL 400/VLM nonlinear aeroelastic toolbox developed at the DLR and, in the case of trim, with linear predictions obtained via MSC.Nastran SOL 144. For the 16-meter wing, matching results in terms of nonlinear aeroelastic static response have been achieved with all the methodologies. For the X-HALE, a close agreement has been found between the present results and the DLR toolbox ones, while slight differences have been observed with UM/NAST. A good agreement between nonlinear and linear trim predictions has been also pointed out due to the moderate deflections experienced by the X-HALE RRV in the examined flight condition. Solution sensitivity to the step size used in the relaxation procedure and to the inertia relief algorithm have been analyzed, showing that computational time can be saved by conveniently setting the number of fluid-structure load steps and by simulating free-free boundary conditions at each iteration of the nonlinear aeroelastic trim loop. Future work will address application the proposed approach to complex FEM models and further investigation on the influence of six degree-of-freedom coupling, load-stepping relaxation, and large-amplitude inertia relief in nonlinear aeroelastic analyses. Comparison with experimental results from the X-HALE RRV flight tests will be carried out to further assess the methodology. The developed nonlinear aeroelastic trim solver will be integrated in an existing FEM-based computational environment for coupled flight dynamics and aeroelastic simulation to extend the toolbox for analysis of very flexible vehicles.

ACKNOWLEDGMENTS

The authors would like to thank the PhD students Patricia Teixeira and Ryan Kitson of the University of Michigan's Active Aeroelasticity and Structures Research Laboratory (A^2SRL) for providing the UM/NAST results.

5 REFERENCES

[1] Noll, T.E., Brown, J.M., Perez-Davis, M.E., Ishmael, S.D., Tiffany, G.C., and Gaier, M., "Investigation of the Helios Prototype Aircraft Mishap," Volume I, January 2004, NASA Mishap Report.

[2] Hodges, D. H., "Geometrically Exact, Intrinsic Theory for Dynamics of Curved and Twisted Anisotropic Beams," *AIAA Journal*, Vol. 41, No. 6, 2003, pp. 1131–1137.

[3] Su, W., and Cesnik, C. E. S., "Strain-based Geometrically Nonlinear Beam Formulation for Modeling Very Flexible Aircraft," *International Journal of Solids and Structures*, Vol. 48, Nos. 16–17, 2011, pp. 2349–2360.

[4] Peters, D. A., and Johnson, M. J., "Finite-State Airloads for Deformable Airfoils on Fixed and Rotating Wings," *Symposium on Aeroelasticity and Fluid/Structure Interaction, ASME Winter Annual Meeting*, edited by P. P. Friedmann and J. C. I. Chang, American Society of Mechanical Engineers, New York, Nov. 1994, pp. 128.

[5] Peters, D. A., Karunamoorthy, S., and Cao, W. M., "Finite State Induced Flow Models Part I: Two-Dimensional Thin Airfoil," *Journal of Aircraft*, Vol. 32, No. 2, 1995, pp. 313–322.

[6] Patil, M.J., and Hodges, D.H., "Flight Dynamics of Highly Flexible Flying Wings," *Journal of Aircraft*, Vol. 43, No. 6, 2006, pp. 1790–1799.

[7] Su, W., and Cesnik, C.E.S., "Nonlinear Aeroelasticity of a Very Flexible Blended-Wing-Body Aircraft," *Journal of Aircraft*, Vol. 47, No. 5, 2010, pp. 1539–1553.

[8] Rodden, W. P., Johnson, E. H., *MSC.Nastran Aeroelastic Analysis User's Guide*, MSC.Software Corporation, Santa Ana, CA, USA, 2010.

[9] Saltari, F., Riso, C., Mastroddi, F., and De Matteis, G., "Finite-Element Based Modeling for Flight Dynamics and Aeroelasticity of Flexible Aircraft," *Journal of Aircraft*, 2017, in publication.

[10] Cavin, R. K. III, and Dusto, A. R., "Hamilton's Principle: Finite-Element Methods and Flexible Body Dynamics," *AIAA Journal* Vol. 15, No. 12, 1977, pp. 1684–1690.

[11] Rodden, W. P., and Love, R. J., "Equations of Motion of a Quasisteady Flight Vehicle Utilizing Restrained Static Aeroelastic Characteristics," *Journal of Aircraft*, Vol. 22, No. 9, 1985, pp. 802–809.

[12] Anon., *MSC.Nastran Linear Statics User's Guide*, MSC.Software Corporation, Santa Ana, CA, USA, 2012.

[13] Anon., *MSC.Nastran Nonlinear Users Guide SOL 400*, MSC.Software Corporation, Santa Ana, CA, USA, 2009.

[14] Katz, J., and Plotkin, A., *Low-Speed Aerodynamics*, Cambridge Aerospace Series, Cambridge University Press, 2001.

[15] Ritter, M., Cesnik, C. E. S., and Kruger, W. R., "An Enhanced Modal Approach for Large Deformation Modeling of Wing-Like Structures," AIAA SciTech, *56th AIAA/ASCE/AHS/ASC Structures, Structural Dynamics, and Materials Conference*, Kissimmee, Florida, 5–9 January 2015.

[16] Ritter, M., Jones, J. R., Cesnik, C. E. S., "Enhanced Modal Approach for Free-Flight Nonlinear Aeroelastic Simulation of Very Flexible Aircraft," AIAA SciTech, *15th Dynamics Specialists Conference*, San Diego, California, 4–8 January 2016.

[17] Anon., *MSC.Nastran Quick Reference Guide Guide*, MSC.Software Corporation, 2012.

[18] Di Vincenzo, F. G., and Castrichini, A., *Hybrid Static Aeroelasticity Toolkit (HSA) User's Guide*, MSC.Software Toulouse, Toulouse, France, 2013.

[19] Cesnik, C. E. S., Senatore, P. J., Su, W., Atkins, E. M., and Shearer, C. M., "X-HALE: A Very Flexible UAV for Nonlinear Aeroelastic Tests," *AIAA Journal*, Vol. 50, No. 12, 2012, pp. 2820–2833.

[20] Jones, J. R., and Cesnik, C. E. S., "Preliminary Flight Test Correlations of the X-HALE Aeroelastic Experiment," *Aeronautical Journal of The Royal Aeronautical Society*, Feb. 2015.

[21] Neto, A. B. G., Silva, R. G. A., Paglione P., and Silvestre F. J., "Formulation of the Flight Dynamics of Flexible Aircraft Using General Body Axes," *AIAA Journal*, Vol. 54, No. 11, 2016, pp. 3516–3534.

COPYRIGHT STATEMENT